Tracking the Precipitation of Sulfate Ions by Hydrocyclone using CFD

Raghad F. Almilly[a]*, Maryam I. Chasib[a], Hiba M. Hashim[b]

[a] University of Baghdad - Department of Chemical Engineering, Iraq
[b] Al-Turath University College - Department of Biomedical Engineering, Iraq
raghad.fareed@coeng.uobaghdad.edu.iq

This research presents a simulation for using the hydrocyclone as a thickener in the precipitation of sulfate ions from waste water as gypsum by CFD – Ansys Fluent 2020. Experimental data of the conditions: inlet flowrates(3 and 11 Lmin-1), inlet concentrations of sulfate ions (100 and 400 mg.L-1) and split ratios (0.1 and 0.9) were adopted from earlier experimental work. Simple theoretical equations were used to model velocity and density for particles precipitation in the hydrocyclone. The simulation tracked the precipitation process. An attempt was made to connect the experimental, simulated and theoretical aspects. It was concluded that Ansys Fluent 2020 was capable to describe the precipitation process. This would be helpful to identify the design and operating conditions.

1. Introduction

Simulation has become an approved method in the engineering and industrial fields due to its saving time, effort, energy and cost.In the field of chemical engineering, there is a lot of research that deals with simulating different processes, especially those that involve fluid flow (Bérard et al., 2019; Antognoli et al., 2019; Zhang et al., 2013). The cyclone is a separation device that induces swirl rotation in a liquid or a gas and therefore imposes an enhanced radial acceleration on a particulate or liquid suspension for the purpose of separation or classification. Cyclones can be used as particle classifiers, phase separators or thickeners. There are different sectors for the application of cyclones such as: mineral processing, oil industry and cement industry. Waste water treatment plants (WWTPs) are the newest sector for cyclones, hydrocyclones applications. Bhaskar and coworkers (Bhaskar et al., 2007) developed a methodology for simulating the performance of hydrocyclone. Initial work included comparison of experimental and simulated results generated using different turbulence models i.e., standard k–ε, k–ε RNG and RSM. Among the three modeling methods, predictions using RSM model were found the best in agreement with experimental results. Waste water holding a big amount of solids has higher density and viscosity than pure water (Narasimha et al., 2014). When a radial acceleration is imposed on waste water the separation of solids is enhanced. Murthy and Bhaskar (Murthy and Bhaskar, 2012) used Eulerian primary phase flow field generation through steady state simulation using RSM turbulence modeling. They evaluated the particle distribution through discrete phase modeling using particle injection technique. The velocity profile and separation efficiency curves of a hydrocyclone were predicted by Euler-Euler approach using CFD (Azimian and Bart, 2016). This approach was found to be capable of considering the particle-particle interactions in highly laden liquid-solid mixtures. Durango-Cogollo and coworkers (Durango-Cogollo et al. 2020) used three known computational turbulence models RNG k- ε , RSM and LES to study the performance of the hydrocyclone. It was found that RSM could reproduce most of the flow patterns of the continuous phase at a relatively low computational cost and time consuming. The present work aims to simulate the experimental data obtained by using hydrocyclone as a thickener to concentrate a pollutant , sulfate ions as gypsum , in the underflow. The suspension behavior was detected by obtaining the contours of the three velocity components, axial, radial and tangential to investigate the flow fields in these directions. Also, the density distribution of the suspension was followed in order to understand the precipitation characteristics. Through these characteristics the design and operating features could be identified.

2. Simulation

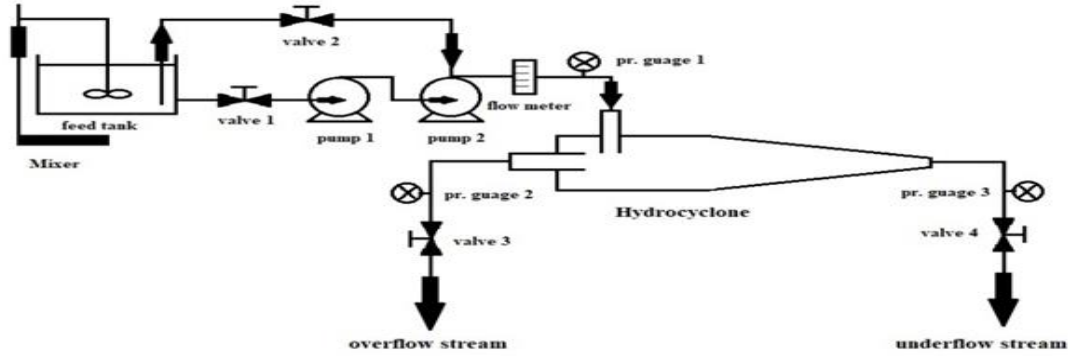The experimental set up is illustrated in Figure 1. The dimensions of the hydrocyclone are illustrated in Table1.

Figure 1: The hydrocyclone layout (Chasib and Almilly, 2019).

Table 1: The hydrocyclone dimensions (Chasib and Almilly, 2019).

Dimension	Hydrocyclone diameter	Inlet diameter	Overflow diameter	Underflow diameter	Cylindrical section length	Conical section length	Vortex finder length	Angle of cone	Thickness
Value (cm)	4	0.57	0.8	1	8	9	1.3	9°	1

Ansys Fluent 2020 was used to perform the hydrocyclone geometry and meshing. The best choice of the cell configuration was tetrahedron to represent the hydrocyclone with 1415692 cells. The governing equation for the numerical solution of three-dimensional hydrocyclone is the equation of change (Bird et al., 2005).

At steady state $(\nabla . \rho \bar{v}) = 0$ (1)

Where: $\bar{v}$ is the time-smoothed velocity of steadily driven turbulent flow (independent on time).

or $\rho \nabla \bar{v} + \bar{v} \nabla \rho = 0$ (2)

So $\bar{v} = - \frac{\nabla \bar{v}}{\nabla \rho} \rho$ (3)

The momentum equation in terms of time-smoothed velocity :

$\frac{\partial}{\partial t} \rho \bar{v} = -[\nabla . \rho \bar{v} \bar{v}] - \nabla \bar{p} - [\nabla . (\bar{\tau}^{(v)} + \bar{\tau}^{(t)})] + \rho g$ (4)

At steady state: $0 = -[\nabla . \rho \bar{v} \bar{v}] - \nabla \bar{p} - [\nabla . (\bar{\tau}^{(v)} + \bar{\tau}^{(t)})] + \rho g$ (5)

Equation (3) reveals that the velocity reduces when the density increases (i.e. the solid loading increases). In the light of Stokes law (Bird et al., 2005):

$v_t = \frac{2}{9} \frac{R^2 (\rho_p - \rho) g}{\mu}$ (6)

Where: v_t is the terminal velocity to which the particle reaches in its sedimentation, R is the radius of the particle, ρ_p is the density of individual particle, ρ is the density of fluid, μ is the fluid viscosity and g is the gravitational constant.
If all the quantities in Eq(6) were considered of low-impact on v_t relative to $(\rho_p - \rho)$, an equation like Eq(7) could be written:

$v = k_1 (\rho_p - \rho)$ (7)

Where k₁ is an arbitrary constant. For turbulent flow, $\bar{v}$ could replace v, the suspension density ρ_s replaced the particle density ρ_p , Eq(7) would be:

$\bar{v} = \acute{k}_1 (\rho_s - \rho)$ (8)

A comparison between Eq(8) and (3) gave the anticipation that a linear relationship with negative slope governed Eq(8). Because the swirling action extended longitudinally, it was expected that ρ_s varied with the longitudinal direction, z as a result of particles accumulation. A linear relationship was proposed between $(\rho_s - \rho)$ and z for dilute suspension:

$$\rho_{s-}\rho = k_2\,z \qquad \text{or} \qquad \rho_s = k_2\,z + \rho \tag{9}$$

Where k_2 is an arbitrary constant in the linear relation.
If f is the volume fraction of gypsum particles in the suspension, then

$$\rho_s = \rho_{gyp}\,f + \rho \tag{10}$$

Where: ρ_{gyp} is the density of gypsum $\rho_{gyp} = 2.32\,g.cm^{-3}$ (Thoeny, 2020). From the definition

$$f = \frac{c \times 10^{-6}}{2.32} \tag{11}$$

Where c is the concentration of gypsum in the suspension in mg.L^{-1}.
Substituting equation (11) into equation (10) yields(in SI units):

$$\rho_s = c \times 10^{-3} + 1000 \tag{12}$$

Gypsum is of limited solubility in water (0.0147 to 0.0182 M at 25 °C) (Lebedev and Kosorukov, 2017) so the suspension reached saturation between sulfate ions and gypsum particles readily. Intuitively there was a position, z_s on the axial direction of the hydrocyclone where the saturation and precipitation occurred. This position was of important consideration in that it determined the required distance for gypsum to precipitate at certain design characteristics and operating conditions.

2.1 Algorithm

An algorithm was used to converge to steady-state.The temperature was kept constant at room temperature.The relationship between the suspension density and the longitudinal dimension of the hydrocyclone, z (Eq(9))was found by drawing the experimental resuls in Excel Microsoft. The experimental values of the suspension density ρ_s can be evaluated at the inlet and outlet of the hydrocyclone using Eq(12). Equation(9) was inserted as a user defined function (UDF) in the algorithm by DEFINE_PROFILE(cell_density, cell, thread) .This was done with the aid of C^{++} computer language. A UDF saved for application when the density was requested by the program.
After determination the suspension density, Reynolds Stress Model (RSM) turbulent model was chosen because of its close representation of the flow in the hydrocyclone (Narasimha et al., 2007). The linear pressure strain was adopted. The boundary conditions were determined by inserting the experimental inlet velocity.The outlet boundary condition was the atmospheric pressure.
The solution was performed by solution control monitors, then initialized with wall-model space to be inlet. After performing the calculations and residuals were convergent, different contour planes were obtained.

3. Results and Discussion

The suspension density ρ_s can be evaluated at the inlet and outlet of the hydrocyclone using equation (12) by inserting the experimental inlet and outlet concentrations of sulfate ions (100 and 400 mg.L^{-1}) , respectively. Getting two values of ρ_s a straight line was drawn between ρ_s and z (0 at the inlet and 0.17 m at the outlet).An equation was determined by Excel as follows:

$$\rho_s = 22.941\,z + 1000.4 \tag{13}$$

This equation was inserted in the algorithm as a variable density of the suspension. The density difference at the inlet and the outlet can be calculated using equation (9). The velocity was related to the density difference by a linear relationship. The velocity was drawn against the density difference depending on the two known points, the entry and the exit of the hydrocyclone. The two points were adequate to represent a linear relationship. The density increased along the hydrocyclone as a result of the accumulation of coarse and heavy particles in the underflow stream by the action of the free vortex. The velocity decreased because of the wall friction. So the equation obtained was of negative slope:

$$\bar{v} = -1.2436\,(\rho_s - \rho) + 7.6814 \tag{14}$$

Figures (2–5) illustrate the contours of velocity, axial velocity, radial velocity, tangential velocity and density along the hydrocyclone during the precipitation of gypsum. It was noticed that the maximum velocity was at the inlet. The inlet diameter of the hydrocyclone controlled the injection rate of momentum. Small inlet diameter offered good separation as a result of increasing the centrifugal force and vice versa (Ni et al., 2018).

The experimental inlet velocity was 7.184 m.s^{-1} which corresponded 11 L.min^{-1} inlet flowrate. The velocity decreased abruptly to the underflow outlet which had an experimental value 2.334 m.s^{-1}. The effect of the entrance to the hydrocyclone persisted most of the cylindrical section as it is illustrated in Figure 2 a. There was a clear flow field of moderate velocity in the cylindrical section resulting from the dissipation of energy of rotation as a result of friction. The length of the cylindrical section had a reversible effect on the separation efficiency (Young et al., 1994). The velocity at the overflow decreased gradually differently from the underflow. This was because the overflow outlet flowrate was only (0.1) of the inlet value for the specified split ratio. The axial velocity was approximately homogeneous throughout the hydrocyclone as it is illustrated in Figure 2 b. It was of moderate value up to the conical section where it decreased gradually and took negative values because of the reverse flow resulted from the air core. At the overflow the velocity was higher. This might be attributed to the accumulation of gypsum in the underflow stream which made the suspension denser and slower than the overflow in addition to the effect of the air core.
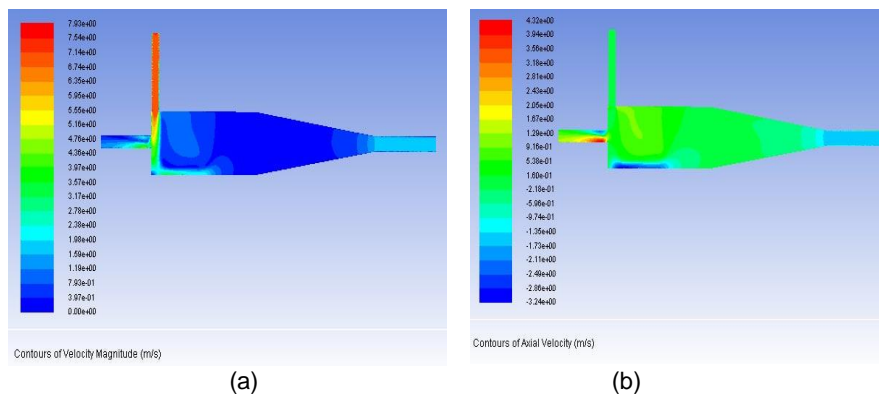

Contours of Velocity Magnitude (m/s)   Contours of Axial Velocity (m/s)

(a)   (b)

Figure 2: The velocity variation in the hydrocyclone, (a) inlet velocity. (b) axial velocity for the conditions: inlet flowrate 11 L.min^{-1}, inlet concentration 400 mg.L^{-1}, split ratio 0.9.

The radial velocity showed approximately a symmetrical variation around the axis of the hydrocyclone as illustrated in Figure 3 a. The radial velocity was of lesser value than the axial velocity component. This was in agreement with Svarovsky (Svarovisky, 2000). The radial velocity at the overflow was higher than the underflow. The tangential velocity is represented in Figure 3 b. It was noticed that it was homogeneous which provided positions of continuous vortices about the axis of the hydrocyclone. The tangential velocity was not influenced by the axial location and this was in agreement with Marthinussen (Marthinussen, 2011). The detection of suspension density is illustrated in Figure 4 a. It could be noticed the increase of the density with the axial dimension of the hydrocyclone according to equation (13). At the underflow the density was maximum. The overflow was less denser because it loaded with finer and lighter particles. The axial position at which the suspension was saturated with sulfate ions could be found by inserting c= 2000 mg.L^{-1}(the saturation concentration) (Runtti et al., 2018) into equation (12) getting ρ_s=1002 Kg.m^{-3}.This value corresponded to the axial location z_s which can be calculated from equation (13) which yields z = 0.0697 ~ 0.07 m. This value of z is very close to the border line between the cylindrical and conical sections (8 cm or 0.08 m). It was obvious from the density contour that saturation occurred at this point. Similarly, the location of saturation was detected at different conditions by changing the inlet flowrate, the inlet sulfate ions concentration and the split ratio. The most important outcome in this research was the determination of the axial location of the onset of precipitation and its dependence upon different operating conditions. When the inlet flowrate was 3 L.min^{-1} (as illustrated in Figure 4 b) the onset of precipitation occurred at the lower half of the conical section near the outlet. This was because of lower flowrate, lower tangential velocity and centrifugal force. In Figure 5 a when the inlet concentration was 100 mg.L^{-1} the precipitation began at the upper half of the conical section because of the very diluted inlet concentration of sulfate ions. It was noticed that the saturation occupied a broader range of axial length due to lower quantity of particles that made their accumulation difficult. Figure 5 b revealed that the onset of precipitation occurred at the conical section within the upper half as a result of using low split ratio, 0.1. The effect of lowering the inlet flowrate was the most influencing than lowering the inlet concentration or lowering the split ratio. From this argument it was concluded that the best location for precipitation was at the cylindrical section. This prevented the particles from raising with the air core back to the overflow.
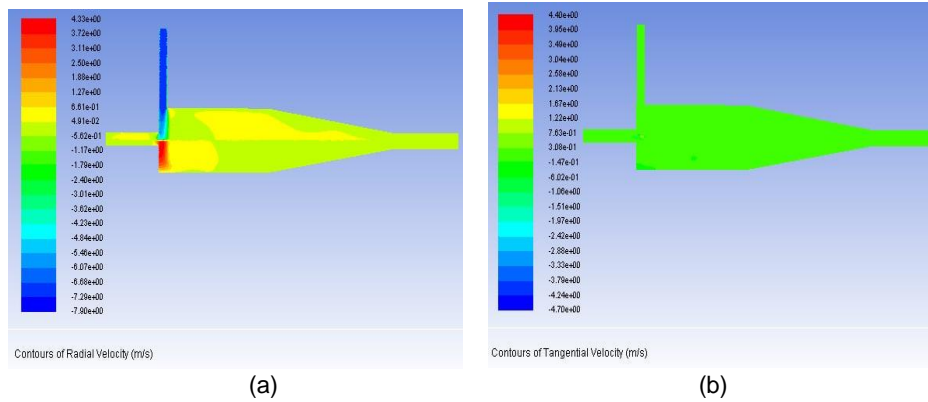
(a)   (b)

Figure 3: The radial velocity variation (a) and the tangential velocity (b) in the hydrocyclone for inlet flowrate 11 L.min^{-1}, ci 400 mg.L^{-1}, split ratio 0.9 .

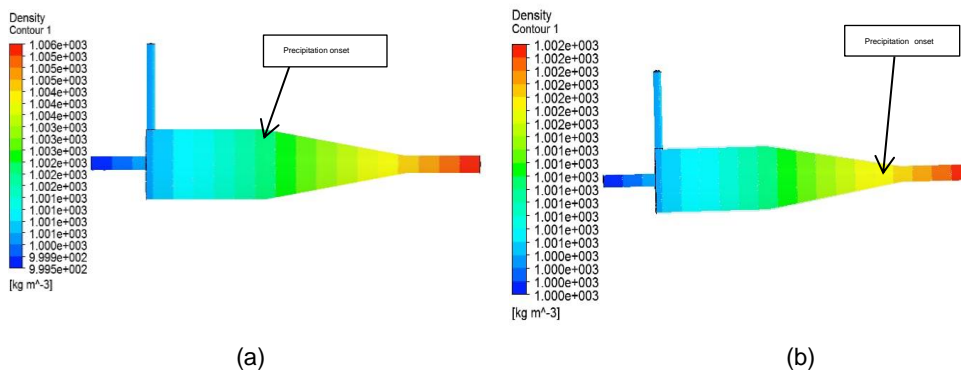(a)   (b)

Figure 4: The density contour in the hydrocyclone, (a) inlet flowrate 11 l.min^{-1}, ci 400 mg.L^{-1}, split ratio 0.9.(b) 3 L.min^{-1}, ci 400 mg.L^{-1} and split ratio 0.9.
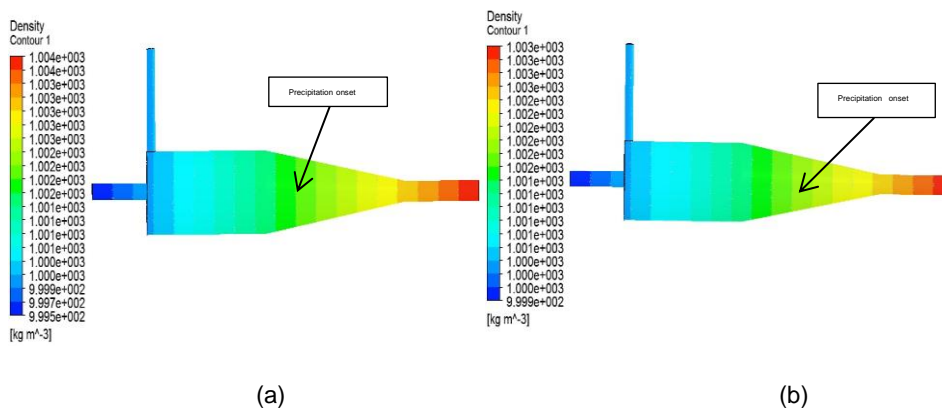

(a)   (b)

Figure 5: Density contour (a) for inlet flowrate 11 L.min^{-1}, ci 100 mg.L^{-1} and split ratio 0.9 and (b) 11 L.min^{-1}, ci 400 mg. L^{-1} and split ratio 0.1.

4. Conclusions

A simulation of the precipitation process of gypsum particles was investigated using experimental data to characterize the details of the process. With the aid of CFD – Ansys Fluent 2020 the experimental data of precipitation at the conditions: inlet flowrate (3 and 11 L.min^{-1}), inlet concentrations of sulfate ions (100 and 400 mg.L^{-1}) and split ratios (0.1 and 0.9) were adopted. Reynolds Stress Model represented the hydrocyclone operation very well. Contours of inlet, axial, radial and tangential velocities as well as the density were

obtained by the simulation. The discussion of these contours revealed the potential use of this scheme in seeking the best operating conditions.

References

Antognoli M., Galletti C., Bacci Di Capaci R., Pannocchia G., Scali C., 2019, Numerical Investigation of the Mixing of Highly Viscous Liquids with Cowles Impellers, Chemical Engineering Transactions, 74, 973-978.

Azimian M., Bart H.-J., 2016, Numerical analysis of hydroabrasion in a hydrocyclone, Pet. Sci., 13, 304–319. Doi: 10.1007/s12182-016-0084-7.

Bérard A., Patience G.S., Blais B., 2019, Experimental methods in chemical engineering: Unresolved CFD-DEM, The Canadian Journal of Chemical Engineering, 98, 424-440.

Bird R.B., Stewart W.E., Lightfoot E.N. (2nd Ed.), 2005, Transport Phenomena, Wiley-India , Delhi. India.

Chasib M., Almilly R., 2019, Designing and studying operational parameters of hydrocyclone for oil – water separation, Association of Arab Universities Journal of Engineering Sciences, 26, 41–51. Doi.org/10.33261/jaaru..26.4.006.

Durango-Cogollo M., Garcia-Bravo J., Newell B., Gonzalez-Mancera A., 2020, CFD Modeling of Hydrocyclones—A Study of Efficiency of Hydrodynamic Reservoirs, fluids, 5, 118. Doi:10.3390/fluids5030118.

Lebedev A. L., Kosorukov V. L., 2017, Gypsum Solubility in Water at 25°C, Geochemistry International, 55, 205–210.

Marthinussen S.-A., 2011, Master Thesis, University of Bergen, Norway.

Narasimha M., Brennan M., Holtham P. N., 2007, A Review of CFD Modelling for Performance Predictions of Hydrocyclone, Engineering Applications of Computational Fluid Mechanics, 1,109–125.

Narasimha M., Mainza A.N., Holtham P.N., Powell M.S., Brennan M. S., 2014, A Semi-Mechanistic Model of Hydrocyclones –Developed from Industrial Data and Inputs from CFD, International Journal of Mineral Processing, 133. Doi:10.1016/j.minpro.2014.08.006.

Ni L., Tian J., Song T., Jong Y., Zhao J., 2018, Optimizing Geometric Parameters in Hydrocyclones for Ethanol Separations, Separation & Purification Reviews, 48, 1-22 . Doi:10.1080/15422119.2017.1421558.

Rama Murthy Y., Udaya Bhaskar K., 2012, Parametric CFD Studies on Hydrocyclone, Powder Technology, 230, 36–47. Doi:10.1016/j.powtec.2012.06.048.

Runtti H., Tolonen E.-T., Tuomikoski S., Luukkonen T., Lassi U., 2018, How to tackle the stringent sulfate removal requirements in mine water treatment—A review of potential methods, Environmental Research, 167, 207–222.

Svarovisky L. (4th Ed.), 2000, Solid liquid separation, Butterworth-Heinemann,Oxford, UK.

Thoeny Z.A., 2020, The Effect of Particle Size Distribution on some Properties of Gypsum, Key Engineering Materials, 857,145-152.

Udaya Bhaskar K., Rama Murthy Y., Ravi Raju M., Sumit Tiwari, Srivastava J.K., Ramakrishnan N., 2007, CFD Simulation and Experimental Validation Studies on Hydrocyclone, Minerals Engineering, 20, 60–71.

Young G.A.B., Wakley W.D., Taggart D.L., Andrew S.L., Worrel J.R., 1994, Oil-Water Separation Using Hydrocyclones: An Experimental Search for Optimum Dimensions, Journal of Petroleum Science and Engineering, 11, 37-50.

Zhang S., Müller D., Arellano-Garcia H, Wozny G., 2013, CFD Simulation of the Fluid Hydrodynamics in a Continuous Stirred-Tank Reactor, Chemical Engineering Transactions, 32, 1441-1446.